atmosphere

MDPI

Article

Origin of Moisture for the Precipitation Produced by the Exceptional Winter Storm Formed over the Gulf of Mexico in March 1993

Patricia Coll-Hidalgo [1,2], Albenis Pérez-Alarcón [1,3] and Luis Gimeno [1,*]

[1] Centro de Investigación Mariña, Environmental Physics Laboratory (EPhysLab), Campus as Lagoas s/n, Universidade de Vigo, 32004 Ourense, Spain; patricia.coll@uvigo.es (P.C.-H.); albenis.perez.alarcon@uvigo.es (A.P.-A.)
[2] Departamento de Meteorología, Empresa Cubana de Navegación Aérea, La Habana 10800, Cuba
[3] Departamento de Meteorología, Instituto Superior de Tecnologías y Ciencias Aplicadas, Universidad de La Habana, La Habana 10400, Cuba
* Correspondence: l.gimeno@uvigo.es

Abstract: On 12–15 March 1993, a severe winter storm (SC93) formed over the Gulf of Mexico, affecting the Caribbean Islands and the eastern coast of the United States (US) and Canada with a notable amount of precipitation, snow and severe local storms. In this study, we investigate the origin of the precipitation generated by SC93 by applying a widely used Lagrangian moisture source diagnostic method. Our findings revealed that most of the moisture came from the western North Atlantic Ocean, the Caribbean Sea and the Gulf of Mexico. Moreover, the eastern US and Mexico acted as notable terrestrial moisture sources. Overall, the moisture contribution from the oceanic origin was higher than the terrestrial counterpart, and the moisture sources progressively shifted northward as the storm moved. In addition, the moisture uptake mainly occurred in the cyclone–anticyclone interaction region.

Keywords: extratropical cyclone; winter storm; moisture sources; precipitation; storm of the century

Citation: Coll-Hidalgo, P.; Pérez-Alarcón, A.; Gimeno, L. Origin of Moisture for the Precipitation Produced by the Exceptional Winter Storm Formed over the Gulf of Mexico in March 1993. *Atmosphere* **2022**, *13*, 1154. https://doi.org/10.3390/atmos13071154

Academic Editor: Chuanfeng Zhao

Received: 22 June 2022
Accepted: 20 July 2022
Published: 21 July 2022

1. Introduction

The winter storms formed over the Gulf of Mexico mainly affect human activity in the southern and eastern United States (US), Florida Peninsula and Caribbean Islands due to, i.e., locally heavy rainfall and the possible occurrence of tornadoes in the squall line [1–4]. One of the most catastrophic winter storms occurred from 12 to 15 March 1993 [4], which is often named "the storm of the century", "Superstorm '93", or "the Great Blizzard of 1993" (hereafter SC93).

The SC93 caused heavy snows exceeding 75 cm in several locations along the eastern coast of North America, with ~90 million people affected in the US [5]; precipitation totals in several regions higher than 2500 mm; tornadoes in northeastern Mexico, Florida and Cuba [1]; and a destructive storm surge in Florida [5]. Approximately 270 deaths were probably caused by the impact of SC93 [5], and about 10 of them were in Cuba [1]. Furthermore, ships and oil rig platforms recorded hurricane-force winds towards the north and northwest of the SC93 centre [5]. Further details of the damages caused by SC93 can be found in Alfonso and Naranjo [1], Kocin et al. [5] and the review of SC93 by the US National Climate Data Center [6].

According to Alfonso and Naranjo [1], SC93 originated from the interaction of a polar flow over the middle US and a low-pressure disturbance over the northern portion of the Gulf of Mexico. By 12 March at 1200 UTC, a deep upper-level trough in the southern part of a polar jet caused the explosive cyclogenesis close to the Texas-Mexican boundary. Additionally, there was a marked gradient between the cold air over the continent and the warm maritime air mass south of the quasi-stationary front. By 13 March at 0000 UTC,

the cold front associated with the southern branch of the polar jet was well marked on the surface, as revealed in the surface charts [5], and the storm continued deepening and moving east-northeastward [1].

Dickinson et al. [2] found that the equivalent potential temperature (θe) increased due to the anomalously warm sea surface temperature in the Gulf of Mexico, favoring the increase of the latent heat release [7]. Consequently, the cyclogenesis and rapid intensification of the storm occurred [7–9]. Bosart et al. [10] and Schultz [11] also highlighted the role played in the extreme cyclogenesis by the deep convection over the Gulf of Mexico and the merger of two troughs into an area influenced by westerly winds; similar to it was described by Hakim et al. [12].

One of the key factors for the occurrence of deep convection is the substantial atmospheric humidity in the lower atmosphere [13–15]. Alfonso and Naranjo [1] found abundant moisture during the explosive cyclogenesis of SC93. Despite the considerable attention received by SC93 in the scientific literature e.g., [1,2,10,11,16], few studies have investigated where the atmospheric moisture came from that favoured explosive cyclogenesis and consequently the extreme total amounts of precipitation.

Therefore, this work aims to apply a Lagrangian moisture tracking method for identifying the origin of moisture that generated the precipitation produced by SC93. This Lagrangian approach has been previously applied, i.e., for investigating the moisture sources for the rainfall of tropical cyclones over the North Atlantic (NATL) basin [17], for identifying the origin of atmospheric humidity for the precipitation produced by the six major hurricanes formed over NATL in 2017 [18] and for studying the sources and transport pathways of deep extratropical cyclones formed in the North Atlantic Ocean [19].

2. Materials and Methods

2.1. Data

To track the SC93 winter storm at a 6-h interval, we used the mean sea level pressure from the ERA-5 reanalysis [20]. The ERA-5 is provided by the European Centre for Medium-Range Weather Forecasts (ECMWF), with $0.25^\circ \times 0.25^\circ$ horizontal resolution and 137 vertical levels. Additionally, we used a three-dimensional wind field, specific humidity and temperature, and two-dimensional 10 m horizontal wind components, large-scale and convective precipitation, 2 m temperature, surface pressure, sensible heat flux and the eastward/northward vertically integrated moisture flux (VIMF) from the ECMWF ERA-Interim reanalysis [21] at $1^\circ \times 1^\circ$ grid spacing and 61 vertical levels. We also used the precipitation records from the Multi-Source Weighted-Ensemble Precipitation (MSWEP) database [22] with $0.1^\circ \times 0.1^\circ$ and 3-hourly spatial and temporal resolutions, respectively.

2.2. Tracking Algorithm

Based on the overview of SC93 by Kocin et al. [5], we delimited the search region by the box extended from 40° W to 120° W and 10° N to 75° N. We tracked SC93 by applying a recent method for tracking tropical cyclones [23] with some minor adjustments. The candidate lows were those in which the MSLP anomaly minima was lower than −3 hPa. The MSLP anomaly ($MSLP_{anom}$) was computed as the difference between MSLP at the analysis time (t) and the average MSLP in the previous 14 days. If the outer radius is lower than 100 km and the MSLP is higher than 1015 hPa, the low is discarded. After findings of the candidate lows in all time steps, the position of a critical centre in the next time step (t + 6) is the nearest low within a 1000 km radius circle. After paring all critical centres, if the duration of the storm is less than 24 h, the track is also discarded.

The outer radius was computed following the methodology proposed by Rudeva and Gulev [24]. The searching of the outer radius starts using a pattern of 36 radial legs from the centre of the critical low with 2000 km of length and spacing at 10 degrees. The critical radius at each leg is located where ΔMSLP computed every 100 km tends to zero. If the previous condition is not satisfied, the critical radius was considered as 2000 km. The minimum MSLP value of all 36 radial legs is taken as the last closed isobar for the low. By

interpolating, we estimated the radial distance of the closed isobar in each radial leg, which determines the geometry of the low, as revealed in the shaded area in Figure 1. The area of that geometry is considered the area of a virtual circumference (see Figure 1), whose virtual radius is assumed as the outer radius.

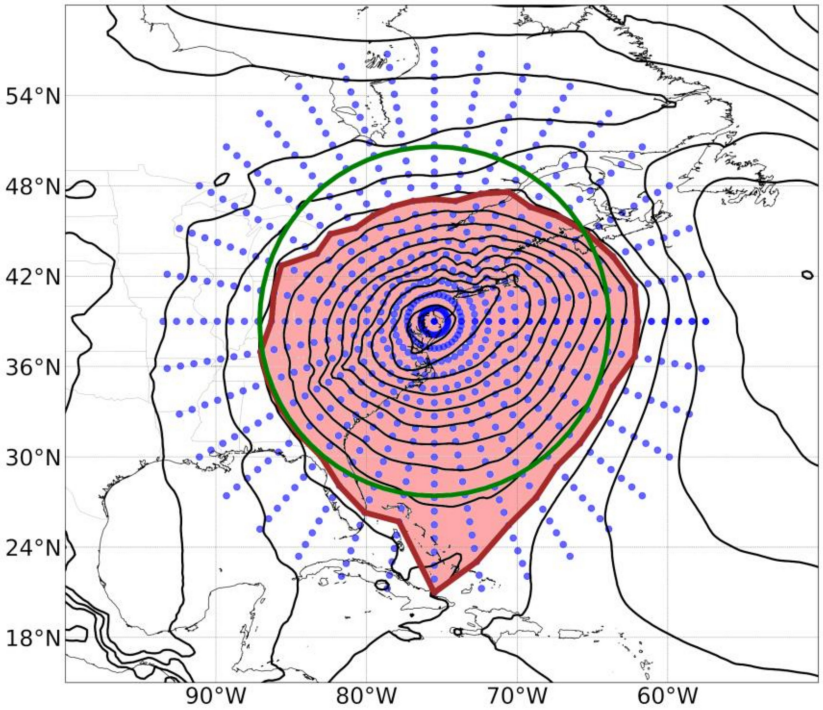

Figure 1. Representation of the outer radius estimates. The black lines represent the isobars, the blue dots denote the radial legs, the brown line represents the geometry of the low (the last closed isobar), the shaded area is the area delimited by the low geometry and the green line is the estimated outer radius.

2.3. Lagrangian Moisture Sources Analysis

We used air parcel trajectories from the Lagrangian FLEXible PARTicle dispersion model (FLEXPART) v9.0 [25]. FLEXPART was forced by the ERA-Interim reanalysis. In the model simulations, the 3D wind field moved about 2 million air parcels with equal mass throughout the atmosphere. While air parcels move in the atmosphere, they could gain or lose moisture by evaporation or precipitation, according to the Lagrangian water budget by Stohl and James [26,27]. It is important to remark that the mixing with adjacent air parcels and the presence of liquid water and ice in the atmosphere are neglected in the Lagrangian approach.

By applying the Lagrangian moisture source diagnostic method proposed by Sodemann et al. [28], the air parcels that precipitated within the area determined by the SC93 size (the target region) at each 6-h time step were followed backwards in time. The precipitant parcels were identified following Läderach and Sodemann [29], and the length of the trajectories of backtracked parcels was 10 days, which is widely used as the lifetime of water vapour in the atmosphere from evaporation to precipitation [30–32]. Precipitation in route can occur during the parcel movement in the atmosphere, then to objectively identify the origin of moisture that precipitated over the SC93 location, the moisture reduction by precipitation before arrive at the target region was discounted in proportion to all previous uptakes.

3. Results and Discussion

3.1. Overview of SC93

Based on the tracking algorithm, SC93 formed on 12 March 1993 at 1200 UTC over the western Gulf of Mexico and dissipated on 15 March 1993 at 1800 UTC south of Greenland. Bergeron [33] proposed the first approach to classify the cyclogenesis of extratropical cyclones but limited to 60° N of latitude. Later, Sanders and Gyakum [34] introduced a scale factor for applying it to all extratropical cyclones. Based on this, SC93 experienced a rapid intensification process. The central pressure firstly decreased by 30 hPa from 12 March at 1200 UTC (Figure 2a) to 13 March 1200 UTC (Figure 2b) when SC93 moved over the warm waters of the Gulf of Mexico [1], and then, the system continued its intensification during the next hours until reached the lowest central pressure of about 961 hPa on 14 March at 0600 UTC. During the unexpected strengthening, SC93 developed a strong squall line and a complex frontal structure that mainly affected the western region of Cuba and Florida with heavy rainfall and the occurrence of severe local storms [1].

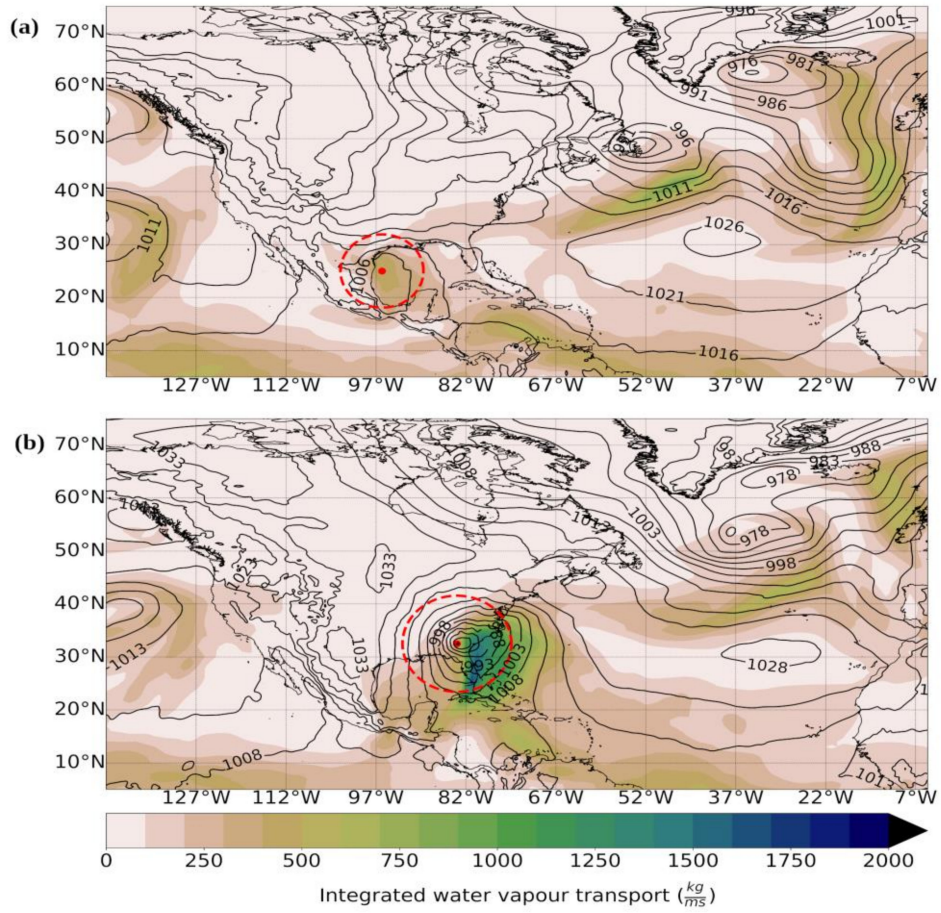

Figure 2. Integrated water vapour transport (shaded) and mean sea level pressure (contours) for (**a**) 12 March 1993 at 1200 UTC and (**b**) 13 March 1993 at 1200 UTC. The red-dashed circles denote the SC93 size, while the position of the storm is marked with a filled square.

Figure 3 depicts the average integrated water vapour transport (IVT) during the SC93 lifetime. It is observed a high moisture transport is parallel to the SC93 trajectory, which favored the highest amount of rainfall and snow recorded over the eastern US and Canada [5]. Based on the finding of Zhang et al. [35], the IVT pattern also suggests that an atmospheric river (AR) acted as a driver of moisture for SC93 during its maximum intensity. Zhang et al. [35] noted that a storm with AR associated has a broad high pressure to its southeast, as shown in Figure 3. During the north-eastward movement, SC93 increased in

size as a consequence of its intensification, confirming the findings of Rudeva [36], who noted that the largest sizes are characteristic of intense cyclones.

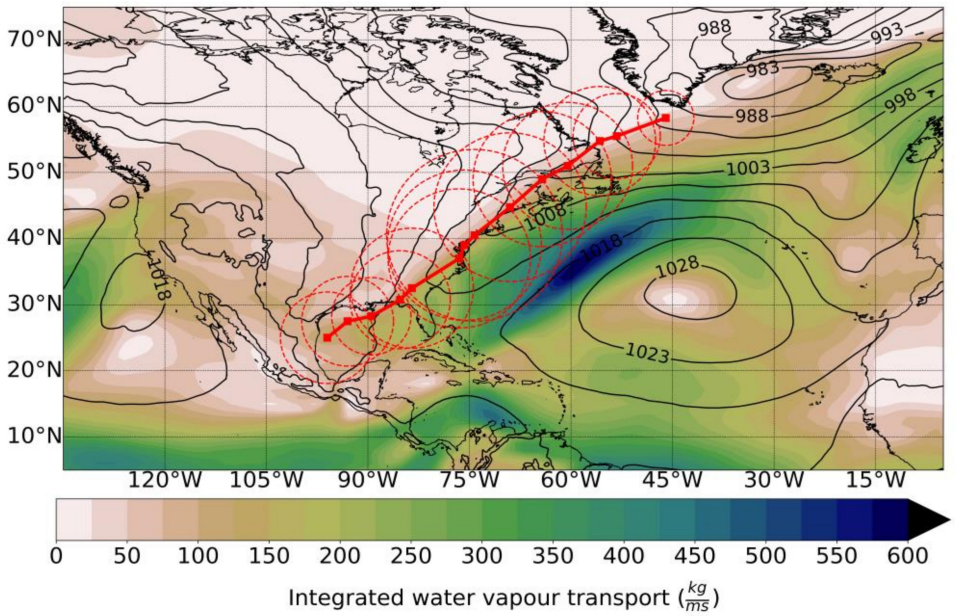

Figure 3. Average integrated water vapour transport (shaded) during the SC93 lifetime and its trajectory (red line). The black lines represent the average sea level pressure and the red-dashed circles denote the SC93 size, while the centre of SC93 every 6 h is marked with a filled square.

As noted in previous works, e.g., [1,5], SC93 produced a higher amount of precipitation along the eastern coast of the US and Canada. Figure 4 displays the accumulated precipitation from 12 March at 1200 UTC to 15 March at 1800 UTC from the MSWEP dataset. Georgia and North and South Carolina achieved the highest amount of precipitation. Nevertheless, the SC93 was not ranked as one of the most extreme precipitation events in the US [37] due to its precipitation occurring over high spatial scales [37], and precipitation records were influenced by the combined effect of winds and snow [38].

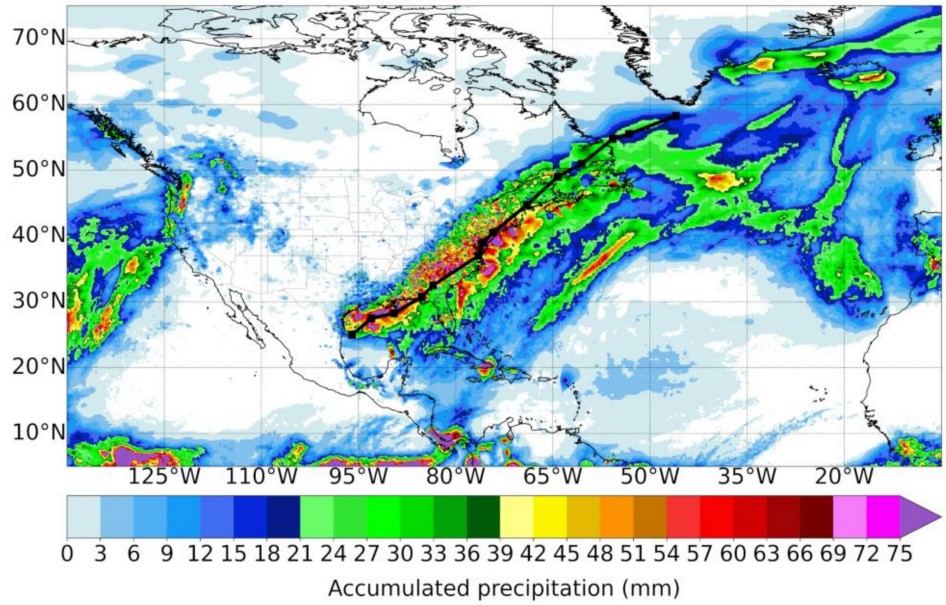

Figure 4. Accumulated precipitation from the Multi-Source Weighted-Ensemble Precipitation dataset from 12 March 1993 at 1200 UTC to 15 March 1993 at 1800 UTC. The black line represents the SC93 trajectory, while the centre of SC93 every 6 h is marked with a filled square.

3.2. Origin of Moisture for the Precipitation Produced by SC93

Next, we discuss the origin of moisture that produced the precipitation associated with SC93 during its lifetime. The moisture sources were identified by applying a Lagrangian moisture source diagnostic method. Figure 5 depicts the trajectories of the air parcels associated with the precipitation of SC93 and the source regions over which they gained moisture. During the genesis phase on 12 March at 1200 UTC, the precipitant moisture mainly was of maritime origin from the Gulf of Mexico and the western Caribbean Sea (Figure 5a). Note also the moisture contribution from terrestrial sources over Mexico. As the storm intensified and moved north-eastward, the sources of moisture for precipitation increased in intensity and extent and progressively moved northward with the cyclone. By 13 March at 1200 UTC, the storm centre was over the southern coast of the US, and the most of moisture came from the western Caribbean Sea, the eastern Gulf of Mexico and the seas surrounding the Bahamas Archipelago (Figure 5c). Likewise, the terrestrial sources of the southeastern United States, the Yucatan Peninsula and the Greater Antilles supplied substantial moisture.

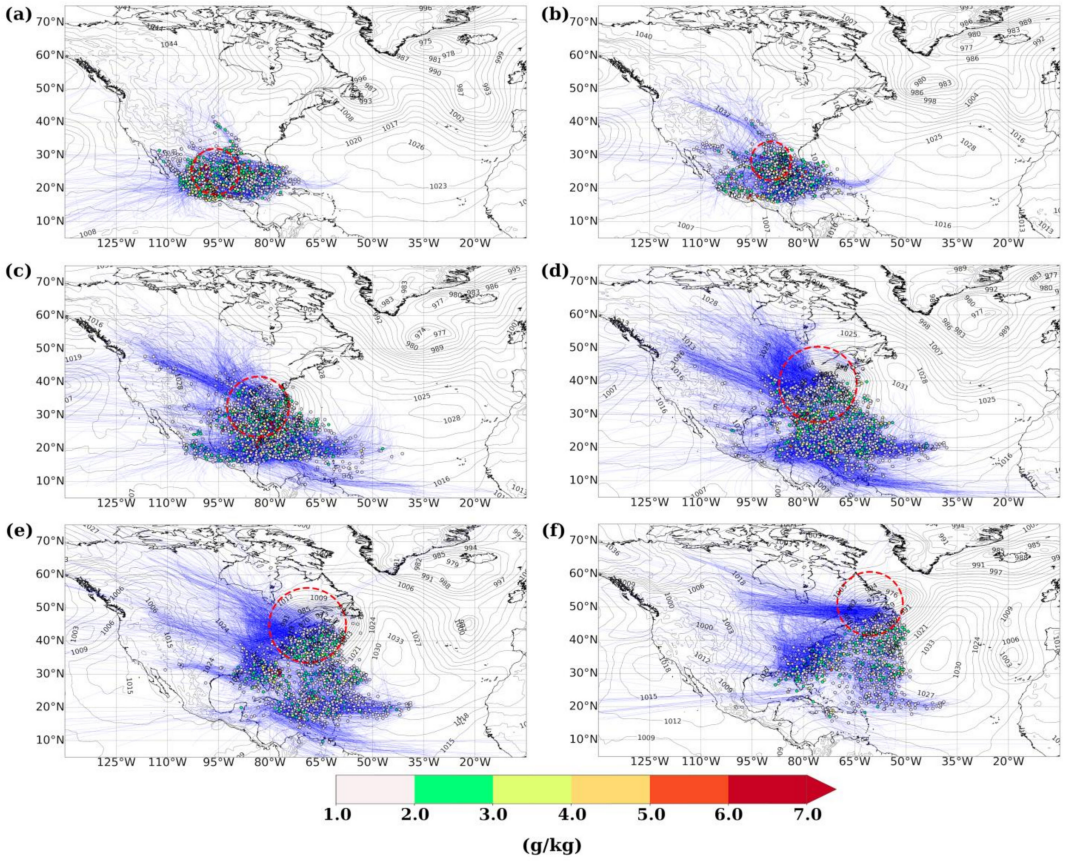

Figure 5. Trajectories associated with SC93 precipitation on (**a**) 12 March at 1200 UTC, (**b**) 13 March at 0000 UTC, (**c**) 13 March at 1200 UTC, (**d**) 14 March at 0000 UTC, (**e**) 14 March at 1200 UTC and (**f**) 15 March at 0000 UTC. Further shown are 6 h changes of specific humidity along trajectories (coloured dots). The mean sea level pressure (hPa) is also plotted in contours and the red-dashed line denotes the SC93 size.

On 14 March 0000 UTC, the storm centre was located over the coast of Virginia. At this time, the western North Atlantic Ocean supplied the highest moisture contribution for the extreme precipitation produced by SC93, followed by the northern Caribbean Sea and the terrestrial source over the southeastern US, as shown in Figure 5d. Lesser moisture was supplied from the tropical North Atlantic Ocean and the Gulf of Mexico. Figure 5e displays the position of SC93 on 14 March at 1200 UTC. Note that the higher moisture contribution

was from the local source located south of the storm centre, close to the eastern coast of the US. Moreover, the western North Atlantic, the Caribbean Sea and terrestrial sources over the eastern US supplied no neglected amount of atmospheric humidity.

The moisture sources decreased in intensity by 15 March 0000 UTC when the storm gradually weakened. From Figure 5f, the moisture uptake pattern exhibited three nuclei. The first was located south of the Gulf of Labrador, the second on the coast of South Carolina and the last, a small nucleus over the central North Atlantic Ocean.

Overall, the footprints of moisture uptakes for the precipitation produced by SC93 shown in Figure 5 agree with Papritz et al. [19]. The most deep moisture uptake occurred in the strengthening phase and declined notably as the storm started to weak. Additionally, moisture contributions from remote locations were small compared with the moisture gained from sources close to the storm centre. Another important finding from Figure 5 is that precipitating moisture often originated in the interaction cyclone–anticyclone region. Papritz et al. [19] linked this moisture uptake with the ascent region of the storm through the so-called feeder airstream.

Additionally, by applying the Lagrangian moisture source diagnostic method, we also computed, following the methodology proposed by Läderach and Sodemann [29], the mean water vapour residence time for the precipitation associated with SC93. On average, the time spent by the air parcels in the atmosphere from evaporation to precipitation was 2.2 ± 0.3 days (uncertainty given as one standard deviation). This result, which agrees with the findings of Papritz et al. [19] for extratropical cyclones and Pérez-Alarcón et al. [17] for tropical cyclones, confirms that the uptakes contributing to precipitation mainly occurred from local sources, as revealed in Figure 5.

Figure 6 summarises the moisture contributions from all sources during the lifetime of SC93. As previously discussed, the higher moisture contribution came from the western North Atlantic Ocean, supplying approximately 39% of total moisture gained by SC93, followed by the Caribbean Sea (~26%), the Gulf of Mexico (~17%), the eastern US (~11%) and Mexico (~7%). Moreover, the VIMF pattern confirms the higher moisture transport was parallel to the storm trajectory and bordering the anticyclone, as shown in Figure 3. Therefore, the main drivers of moisture were the western branch of the high-pressure system and the cyclone-relative flow controlled by the cyclone propagation, in agreement with Papritz et al. [19].

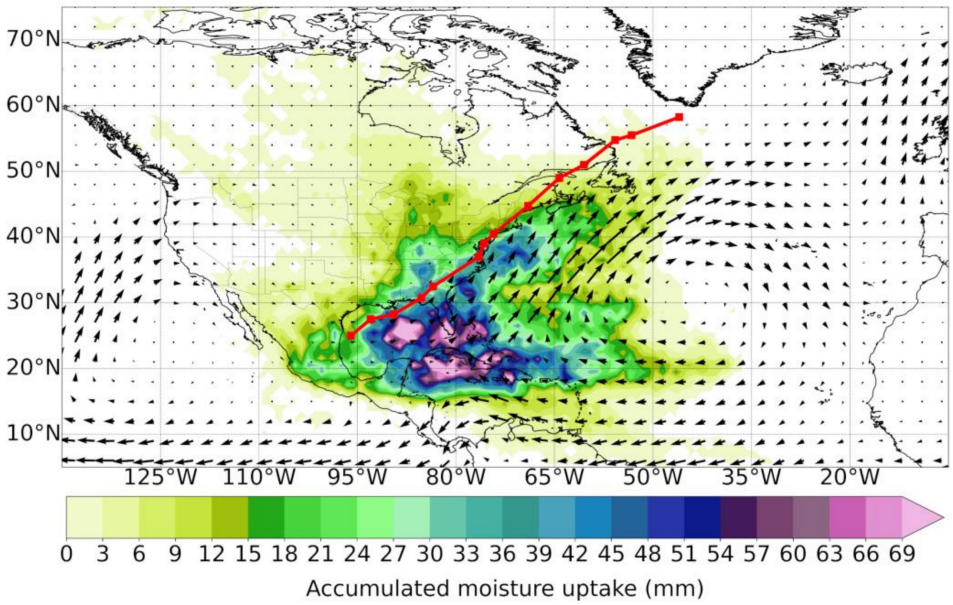

Figure 6. Accumulated moisture uptake (mm) during the SC93 lifetime. The vertically integrated moisture flux is represented by arrows (kg/ms). The red line denotes the SC93 trajectory, while the centre of SC93 every 6 h is marked with a filled square.

We also computed the moisture contribution for the precipitation over land associated with SC93 during its lifetime. To do this, we backtracked the air parcels within the SC93 but residing over land (Figure 7a). The moisture uptake pattern was quite similar to that using the area delimited by the SC93 outer radius (Figure 7b) but less intense. This behaviour was expected due to the smaller target region. Overall, the western North Atlantic supplied ~37% of total moisture uptake, followed by the Gulf of Mexico (~28%) and the Caribbean Sea (~20%). The remaining ~15% came from the terrestrial sources over Mexico and the southeastern US.

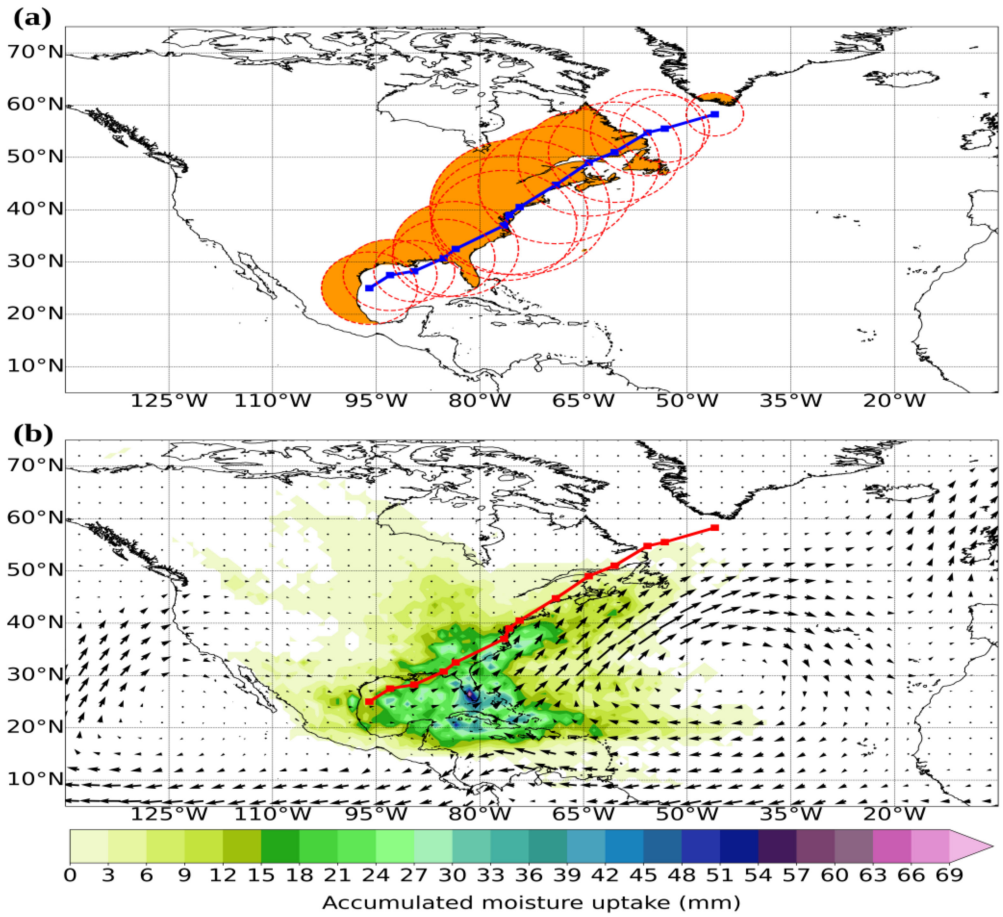

Figure 7. (**a**) Composite of target regions (shaded) to identify the air parcels within the SC93 area that precipitated over land. (**b**) Accumulated moisture uptake (mm) during the SC93 lifetime for the precipitation over land. The vertically integrated moisture flux is represented by arrows (kg/ms). The blue and red lines denote the SC93 trajectory, while the centre of SC93 every 6-h is marked with a filled square. The red-dashed circles in (**a**) denote the SC93 size.

4. Conclusions

The winter storm that originated over the Gulf of Mexico on 12 March 1993, known as the Storm of the Century (SC93), generated a high amount of precipitation along the Caribbean Islands and eastern North America. The SC93 was one of the most intense storms of the twentieth century. This work investigated the origin of moisture that generated the precipitation associated with SC93. This goal was addressed firstly by applying a cyclone detecting and tracking algorithm for the detailed analysis of the SC93 position at the 6-hourly interval and then by using a Lagrangian moisture source diagnostic method to identify the moisture sources. Herein, we used the atmospheric air parcel trajectories from the Lagrangian FLEXible PARTicle dispersion model forced by the ERA-Interim reanalysis.

Our findings demonstrated that the western North Atlantic Ocean provided the highest amount of moisture (~39%) that generated the precipitation related to SC93, followed by

the Caribbean Sea (~26%) and the Gulf of Mexico (~17%). Likewise, the terrestrial source over the eastern United States and Mexico also support substantial atmospheric humidity. The results presented in this study confirmed that the moisture transport from the western Caribbean Sea and the Gulf of Mexico was relevant in the cyclone's explosive development. Overall, the contributions from oceanic sources were higher than from terrestrial sources.

Moreover, moisture sources increased in extent and intensity as SC93 intensified and progressively moved northward with the storm motion. We also found that the moisture uptake was more intense during the intensification and notably decayed during the weakening phase. The cyclone relative flow or the feeder airstream and the western branch of the anticyclone were the main drivers of moisture towards the SC93 positions.

Our findings can contribute to the understanding of moisture transport patterns associated with extratropical cyclones that originate over the Gulf of Mexico. For example, the intense extratropical cyclone Elsa, which formed in this area in December 2019, described during the half part of its lifetime a similar trajectory to the SC93, gaining moisture from the same sources before joining with an intense zonal flow that crossed the entire North Atlantic [39]. The compilation of our results and the findings from previous studies, e.g., [1,2,5,10,11,16], about the dynamic and thermodynamic factors that contributed to the formation of SC93 will allow forecasters to have more complete knowledge about the aspects that favour the occurrence of extreme precipitation associated with this type of storm, and consequently the emission of warning for the reduction of damages.

Additionally, these results are particularly relevant in a warmer climate due to the destructive nature of SC93. The rising sea surface temperature may alter the moisture supply by modifying the position and extension of sources or by inducing changes in the large-scale circulation patterns of the ocean and the atmosphere. Future studies will focus on performing a climatology of the moisture sources for the precipitation associated with unusual cases such as SC93 to improve our understanding of how, among other large-scale and local environmental factors, the moisture uptake can favour the explosive cyclogenesis and rapid intensification of extratropical cyclones. Furthermore, we also will perform in future climatological studies the analysis of the role played by the main modes of climate variability, such as the North Atlantic Oscillation or the El Niño–Southern Oscillation, in the variability of the moisture source regions, as well as a complete evaluation of the moisture transported associated with low-level jets and atmospheric rivers.

Author Contributions: Conceptualization, L.G. and A.P.-A.; methodology, P.C.-H., A.P.-A. and L.G.; software, P.C.-H. and A.P.-A.; validation, P.C.-H. and A.P.-A.; formal analysis, P.C.-H., A.P.-A. and L.G.; investigation, P.C.-H. and A.P.-A.; resources, L.G.; data curation, P.C.-H. and A.P.-A.; writing—original draft preparation, P.C.-H. and A.P.-A.; writing—review and editing, P.C.-H.; A.P.-A. and L.G.; visualization, P.C.-H. and A.P.-A.; supervision, L.G. All authors have read and agreed to the published version of the manuscript.

Funding: This work received financial support from the LAGRIMA and SETESTRELO projects (Grants RTI2018-095772-B-I00 and PID2021-122314OB-I00, respectively) granted by the Ministerio de Ciencia, Innovación y Universidades, Spain. Partial and partial support from the Xunta de Galicia under the Project ED431C 2021/44 (Programa de Consolidación e Estructuración de Unidades de Investigación Competitivas (Grupos de Referencia Competitiva) and Consellería de Cultura, Educación e Universidade).

Institutional Review Board Statement: Not applicable.

Informed Consent Statement: Not applicable.

Data Availability Statement: The ERA-5 reanalysis data set was extracted from https://www.ecmwf.int/en/forecasts/datasets/reanalysis-datasets/era5 (accessed on 14 May 2022), while the ERA-Interim reanalysis was retrieved from https://apps.ecmwf.int/datasets/data/interim-full-daily/levtype=sfc/ (accessed on 5 May 20225). The Multi-Source Weighted-Ensemble Precipitation (MSWEP) dataset is freely available upon request from http://www.gloh2o.org/ (accessed on 20 April 2022). The FLEXPART model can be downloaded from https://www.flexpart.eu/wiki/FpRoadmap (accessed on 18 April 2022).

Acknowledgments: A.P.-A. thanks the University of Vigo for the PhD grant program. This work has been also possible thanks to the computing resources and technical support provided by CESGA (Centro de Supercomputacion de Galicia). The authors acknowledge the Copernicus Climate Change Service for freely providing the ECMWF reanalysis database.

Conflicts of Interest: The authors declare no conflict of interest.

References

1. Alfonso, A.P.; Naranjo, L.R. Genesis and evolution of a severe squall over western Cuba. A case study of March 1993. *Weather Forecast.* **1996**, *11*, 89–102. [CrossRef]
2. Dickinson, M.J.; Bosart, L.F.; Bracken, W.E.; Hakim, G.J.; Schultz, D.M.; Bedrick, M.A.; Tyle, K.R. The March 1993 Superstorm cyclogenesis: Incipient phase synoptic-and convective-scale flow interaction and model performance. *Mon. Weather Rev.* **1997**, *125*, 3041–3072. [CrossRef]
3. Zielinski, G.A. A classification scheme for winter storms in the eastern and central United States with an emphasis on nor'easters. *Bull. Am. Meteorol. Soc.* **2002**, *83*, 37–52. [CrossRef]
4. Changnon, S.A. Catastrophic winter storms: An escalating problem. *Clim. Chang.* **2007**, *84*, 131–139. [CrossRef]
5. Kocin, P.J.; Schumacher, P.N.; Morales, R.F., Jr.; Uccellini, L.W. Overview of the 12–14 March 1993 superstorm. *Bull. Am. Meteorol. Soc.* **1995**, *76*, 165–182. [CrossRef]
6. Lott, N. The Big One! A Review of the March 12–14, 1993 "Storm of the Century". Techincal Report. United States National Climate Data Center. 1993. Available online: https://www1.ncdc.noaa.gov/pub/data/techrpts/tr9301/tr9301.pdf (accessed on 16 June 2022).
7. Liberato, M.L.R.; Pinto, J.G.; Trigo, I.F.; Trigo, R.M. Klaus—An exceptional winter storm over northern Iberia and southern France. *Weather* **2011**, *66*, 330–334. [CrossRef]
8. Liberato, M.L.R.; Pinto, J.G.; Trigo, R.M.; Ludwig, P.; Ordóñez, P.; Yuen, D.; Trigo, I.F. Explosive development of winter storm Xynthia over the subtropical North Atlantic Ocean. *Nat. Hazards Earth Syst. Sci.* **2013**, *13*, 2239–2251. [CrossRef]
9. Fink, A.H.; Brücher, T.; Ermert, V.; Krüger, A.; Pinto, J.G. The European storm Kyrill in January 2007: Synoptic evolution, meteorological impacts and some considerations with respect to climate change. *Nat. Hazards Earth Syst. Sci.* **2009**, *9*, 405–423. [CrossRef]
10. Bosart, L.F.; Hakim, G.J.; Tyle, K.R.; Bedrick, M.A.; Bracken, W.E.; Dickinson, M.J.; Schultz, D.M. Large-scale antecedent conditions associated with the 12–14 March 1993 cyclone ("Superstorm'93") over eastern North America. *Mon. Weather Rev.* **1996**, *124*, 1865–1891. [CrossRef]
11. Schultz, D.M.; Bracken, W.E.; Bosart, L.F.; Hakim, G.J.; Bedrick, M.A.; Dickinson, M.J.; Tyle, K.R. The 1993 superstorm cold surge: Frontal structure, gap flow, and tropical impact. *Mon. Weather Rev.* **1997**, *125*, 5–39. [CrossRef]
12. Hakim, G.J.; Keyser, D.; Bosart, L.F. The Ohio Valley wave-merger cyclogenesis event of 25–26 January 1978. Part II: Diagnosis using quasigeostrophic potential vorticity inversion. *Mon. Weather Rev.* **1996**, *124*, 2176–2205. [CrossRef]
13. Shinoda, T.; Uyeda, H. Effective factors in the development of deep convective clouds over the wet region of eastern China during the summer monsoon season. *J. Meteorol. Soc. Jpn.* **2002**, *80*, 1395–1414. [CrossRef]
14. Xu, X.; Sun, C.; Lu, C.; Liu, Y.; Zhang, G.J.; Chen, Q. Factors affecting entrainment rate in deep convective clouds and parameterizations. *J. Geophys. Res. Atmos.* **2021**, *126*, e2021JD034881. [CrossRef]
15. Feng, Z.; Varble, A.; Hardin, J.; Marquis, J.; Hunzinger, A.; Zhang, Z.; Thieman, M. Deep Convection Initiation, Growth, and Environments in the Complex Terrain of Central Argentina during CACTI. *Mon. Weather Rev.* **2022**, *150*, 1135–1155. [CrossRef]
16. Caplan, P.M. The 12–14 March 1993 superstorm: Performance of the NMC global medium-range model. *Bull. Am. Meteorol. Soc.* **1995**, *76*, 201–212. [CrossRef]
17. Pérez-Alarcón, A.; Sorí, R.; Fernández-Alvarez, J.C.; Nieto, R.; Gimeno, L. Where does the moisture for North Atlantic tropical cyclones come from? *J. Hydrometeorol.* **2022**, *23*, 457–472. [CrossRef]
18. Pérez-Alarcón, A.; Coll-Hidalgo, P.; Fernández-Alvarez, J.C.; Sorí, R.; Nieto, R.; Gimeno, L. Moisture sources for precipitation associated with major hurricanes during 2017 in the North Atlantic basin. *J. Geophys. Res. Atmos.* **2022**, *127*, e2021JD035554. [CrossRef]
19. Papritz, L.; Aemisegger, F.; Wernli, H. Sources and transport pathways of precipitating waters in cold-season deep North Atlantic cyclones. *J. Atmos. Sci.* **2021**, *78*, 3349–3368. [CrossRef]
20. Hersbach, H.; Bell, B.; Berrisford, P.; Hirahara, S.; Horányi, A.; Muñoz-Sabater, J.; Nicolas, J.; Peubey, C.; Radu, R.; Schepers, D.; et al. The ERA5 global reanalysis. *Q. J. R. Meteorol. Soc.* **2020**, *146*, 1999–2049. [CrossRef]
21. Dee, D.P.; Uppala, S.M.; Simmons, S.J.; Berrisford, P.; Poli, P.; Kobayashi, S.; Andrae, U.; Balmaseda, M.A.; Balsamo, G.; Bauer, P.; et al. The ERA-Interim reanalysis: Configuration and performance of the data assimilation system. *Q. J. R. Meteorol. Soc.* **2011**, *137*, 553–597. [CrossRef]
22. Beck, H.E.; van Dijk, A.I.; Larraondo, P.R.; McVicar, T.R.; Pan, M.; Dutra, E.; Miralles, D.G. MSWX: Global 3-Hourly 0.1° Bias-Corrected Meteorological Data Including Near-Real-Time Updates and Forecast Ensembles. *Bull. Am. Meteorol. Soc.* **2022**, *103*, E710–E732. [CrossRef]

23. Bacmeister, J.T.; Suarez, M.J.; Robertson, F.R.; Wehner, M.F.; Neale, R.B.; Gettelman, A.; Hannay, C.; Lauritzen, P.H.; Caron, J.M.; Truesdale, J.E. Exploratory high-resolution climate simulations using the Community Atmosphere Model (CAM). *J. Clim.* **2014**, *27*, 3073–3099. [CrossRef]
24. Rudeva, I.; Gulev, S.K. Climatology of cyclone size characteristics and their changes during the cyclone life cycle. *Mon. Weather Rev.* **2007**, *135*, 2568–2587. [CrossRef]
25. Stohl, A.; Forster, C.; Frank, A.; Seibert, P.; Wotawa, G. Technical note: The Lagrangian particle dispersion model FLEXPART version 6.2. *Atmos. Chem. Phys.* **2005**, *5*, 2461–2474. [CrossRef]
26. Stohl, A.; James, P.A. Lagrangian analysis of the atmospheric branch of the global water cycle. Part I: Method description, validation, and demonstration for the August 2002 flooding in central Europe. *J. Hydrometeorol.* **2004**, *5*, 6562–6678. [CrossRef]
27. Stohl, A.; James, P.A. Lagrangian analysis of the atmospheric branch of the global water cycle. Part II: Moisture transports between the Earth's ocean basins and river catchments. *J. Hydrometeorol.* **2005**, *6*, 961–984. [CrossRef]
28. Sodemann, H.; Schwierz, C.; Wernli, H. Interannual variability of Greenland winter precipitation sources: Lagrangian moisture diagnostic and north Atlantic oscillation influence. *J. Geophys. Res.* **2008**, *113*, D03107. [CrossRef]
29. Läderach, A.; Sodemann, H. A revised picture of the atmospheric moisture residence time. *Geophys. Res. Lett.* **2016**, *43*, 924–933. [CrossRef]
30. Numaguti, A. Origin and recycling processes of precipitating water over the Eurasian continent: Experiments using an atmospheric general circulation model. *J. Geophys. Res.* **1999**, *104*, 1957–1972. [CrossRef]
31. van der Ent, R.J.; Tuinenburg, O. The residence time of water in the atmosphere revisited. *Hydrol. Earth Syst. Sci.* **2017**, *21*, 779–790. [CrossRef]
32. Gimeno, L.; Eiras-Barca, J.; Durán-Quesada, A.M.; Dominguez, F.; van der Ent, R.; Sodemann, H.; Sánchez-Murillo, R.; Nieto, R.; Kirchner, J.W. The residence time of water vapour in the atmosphere. *Nat. Rev. Earth Environ.* **2021**, *2*, 558–569. [CrossRef]
33. Bergeron, T. Reviews of modern meteorology-12: The problem of tropical hurricanes. *Q. J. R. Meteor. Soc.* **1954**, *80*, 131–164. [CrossRef]
34. Sanders, F.; Gyakum, J.R. Synoptic-dynamic climatology of the "bomb". *Mon. Weather Rev.* **1980**, *108*, 1589–1606. [CrossRef]
35. Zhang, Z.; Ralph, F.M.; Zheng, M. The relationship between extratropical cyclone strength and atmospheric river intensity and position. *Geophys. Res. Lett.* **2019**, *46*, 1814–1823. [CrossRef]
36. Rudeva, I.A. On the relation of the number of extratropical cyclones to their sizes. *Izv. Atmos. Ocean Phys.* **2008**, *44*, 273–278. [CrossRef]
37. Konrad, C.E. The most extreme precipitation events over the eastern United States from 1950 to 1996: Considerations of scale. *J. Hydrometeorol.* **2001**, *2*, 309–325. [CrossRef]
38. Legates, D.R.; DeLiberty, T.L. Measurement biases in the United States rain gauge network. *J. Am. Water Resour. Assoc.* **1993**, *29*, 855–861. [CrossRef]
39. Stojanovic, M.; Gonçalves, A.; Sorí, R.; Vázquez, M.; Ramos, A.M.; Nieto, R.; Gimeno, L.; Liberato, M.L.R. Consecutive Extratropical Cyclones Daniel, Elsa and Fabien, and Their Impact on the Hydrological Cycle of Mainland Portugal. *Water* **2021**, *13*, 1476. [CrossRef]